International Journal of Fracture 38: 295–310 (1988)

Theory and analysis of deformation moment tensor due to microcracking

M. ENOKI and T. KISHI
Research Center for Advanced Science and Technology, University of Tokyo, 4-6-1 Komaba, Meguro-ku, Tokyo 153, Japan

Received 2 March 1988; accepted 10 June 1988

Abstract. The method to represent a general infinitesimal deformation as a deformation moment tensor is proposed and the physical meaning of deformation moment tensor in the case of microcracking is made clear. Developing the measuring and analysis system for acoustic emission waveform analysis, these moment tensor components due to microcracking can be determined experimentally. The remarkable method in this study is established to evaluate the moment tensor with the dynamic Green's function of finite media by computer simulation due to finite difference method and the iterative deconvolution with multiple Green's function.

Applying the present method to fracture toughness testing for ASTM A470 steel, moment tensor of quasi-cleavage facet within the plastic zone near the tip of the pre-crack was obtained from the six channels' acoustic emission waveform analysis. In addition to three-dimensional location of these microcracks, fracture mode and quantitative size of microcracks can be estimated from the obtained moment tensor.

1. Introduction

Fracture criteria and phenomena in materials can be understood generally by macroscopic fracture mechanics [1]. However, fracture process in materials is a heterogeneous phenomenon in time and space, which essentially depends on both the inhomogeneity of materials and the applied stress state. It is recognized that in ductile materials the nucleation, growth and coalescence of voids control fracture processes [2–4], while in brittle materials local cleavage facets and/or transgranular cracks are ultimately responsible for fracture [5]. So in any fracture process, to understand a characteristic of microcracks related to microstructure is a fundamental step to understanding fracture mechanism.

On the other hand, many kinds of toughening techniques have been proposed according to the strong claim for high toughness materials [6]. In the case of ceramics, which do not include plastic deformation, microcracks nucleated at the process zone near the crack tip can relax the stress concentration and enhance the fracture toughness [7, 8], which is so called as a microcrack toughening. Thus in any case for the purpose of understanding both fracture mechanism and toughening mechanism, it is necessary to establish the method to quantitatively evaluate microcracks. However at present even the parameters which represent microcracks universally have not been established.

In the fields of micromechanics and seismology, the deformations, such as the above mentioned microcracks have been formulated analytically. Those deformations in materials can be generally represented as nonelastic "eigenstrain" in micromechanics; which is a mechanics to treat mechanical behaviors of continua elasticity [9]. In this treatment many researchers have investigated the static eigenstrain, but so far the dynamic eigenstrain, that

is the generation of eigenstrain, has not been so well studied. Although the seismology has the similar concept of "seismic moment", this parameter has not been directly connected with the fracture problem in materials. So the relationship between microcracking and eigenstrain (or seismic moment) has to be established and then the method to obtain these seismic moments has to be developed, because so far eigenstrain and seismic moment due to microcracking have not been determined experimentally.

Acoustic emission (AE) technique has been used as an almost unique method to detect dynamic deformation and fracture of materials with high sensitivity. Because AE signals were not exact in the treatment of mechanics, a few studies [10–14] have attempted to characterize acoustic emission sources quantitatively on the analogy of seismology [15].

In the present paper, firstly we represent an infinitesimal deformation in materials as a dynamic eigenstrain and propose the deformation moment tensor as the physical quantity to uniqely describe such a deformation. Secondly, we make clear the physical meaning of deformation moment tensor due to microcracking in materials, which is a typical example of an infinitesimal deformation. At last developing the experimental and analysis method to determine the moment tensor due to microcracking experimentally in accordance with the AE method, we obtain the moment tensor components and quantitatively evaluate each microfracture characteristic, such as size, fracture mode and nucleation rate of each microcrack.

2. Theory

2.1. Eigenstrain and deformation moment tensor

Let V denote an elastic domain occupied by a given three-dimensional body and $\varepsilon^*_{mn}(\mathbf{x}, t)$ denote an eigenstrain tensor in V. Then we can state the displacement field due to $\varepsilon^*_{mn}(\mathbf{x}, t)$ as [9]

$$u_i(\mathbf{x}', t) = \int_V C_{jkmn}\varepsilon^*_{mn}(\mathbf{x}, t) * G_{ij,k}(\mathbf{x}', \mathbf{x}, t)\, \mathrm{d}V(\mathbf{x}), \tag{2.1}$$

where C_{jkmn} is the elastic stiffness tensor, $G_{ij}(\mathbf{x}', \mathbf{x}, t)$ is the displacement field in the direction x_i at position $\mathbf{x}'$ at the time t due to an impulsive force in the direction x_j at $\mathbf{x}$ at time 0. The comma indicates a differentiation and $*$ means a convolution integral with respect to time. If the dimension of region occupied by eigenstrain $\varepsilon^*_{mn}(\mathbf{x}, t)$ is small compared with the distance between the position $\mathbf{x}$ and $\mathbf{x}'$, and the shortest wavelength due to $\varepsilon^*_{mn}(\mathbf{x}, t)$, then the point source approximation is applied. We can finally state the displacement field due to eigenstrain as

$$u_i(\mathbf{x}', t) = G_{ij,k}(\mathbf{x}', \mathbf{x}, t) * D_{jk}(\mathbf{x}, t), \tag{2.2}$$

where deformation moment tensor $D_{jk}(\mathbf{x}, t)$, which is the quantity to present an infinitesimal deformation, is defined as

$$\begin{aligned} D_{jk}(\mathbf{x}, t) &= \int_V C_{jkmn}\varepsilon^*_{mn}(\mathbf{x}'', t)\, \mathrm{d}V(\mathbf{x}'') \\ &= C_{jkmn}\varepsilon^*_{mn}(\mathbf{x}, t)\, \mathrm{d}V, \end{aligned} \tag{2.3}$$

and dV is the volume of deformation domain. Deformation moment tensor $D_{jk}(\mathbf{x}, t)$ is a symmetry tensor of a second order, which is represented by mode and intensity of an infinitesimal deformation.

For isotropic materials, C_{jkmn} can be written as

$$C_{jkmn} = \lambda\delta_{jk}\delta_{mn} + \mu(\delta_{jm}\delta_{kn} + \delta_{jn}\delta_{km}), \tag{2.4}$$

where λ and μ are the Lamé's constants, and δ_{jk} is the Kronecker's delta. We substitute (2.4) into (2.3) and find

$$D_{jk}(\mathbf{x}, t) = (\lambda\varepsilon^*_{mm}\delta_{jk} + 2\mu\varepsilon^*_{jk})\, dV. \tag{2.5}$$

Equation (2.5) shows that independent six quantities of D_{jk} are represented by seven quantities of ε^*_{mn} and dV. Let us consider the eigenvalue problem of D_{jk} because D_{jk} is a symmetry tensor of a second order. We can calculate three invariants J_1, J_2 and J_3 respectively

$$\begin{aligned}
J_1 &= D_{ii} = (3\lambda + 2\mu)\varepsilon^*_{ii}\, dV, \\
J_2 &= [(3\lambda^2 + 4\lambda\mu + 2\mu^2)(\varepsilon^*_{ii})^2 - 2\mu^2(\varepsilon^*_{ij}\varepsilon^*_{ij})]\, (dV)^2, \\
J_3 &= (1/3)[3\lambda^3 + 6\lambda^2\mu + 6\lambda\mu^2 + 4\mu^3)(\varepsilon^*_{ii})^3 - (6\lambda\mu^2 + 12\mu^3)\varepsilon^*_{kk}(\varepsilon^*_{ij}\varepsilon^*_{ij}) \\
&\quad + 8\mu^3\varepsilon^*_{ij}\varepsilon^*_{jk}\varepsilon^*_{ki}]\, (dV)^3.
\end{aligned} \tag{2.6}$$

Eigenvalues D are three solutions of the following equation,

$$D^3 - J_1D^2 + J_2D - J_3 = 0. \tag{2.7}$$

2.2. Generation of microcracks

It is well known that the generation of microcracks can be modeled as the discontinuity of displacement on the faulting surface like a dislocation [15–18]. Plastic distortion $\beta^*_{ji}(\mathbf{x}, t)$ due to this discontinuity of displacement $[\mathbf{u}(\mathbf{x}, t)]$ on a surface A, which is shown in Fig. 1, can be represented as

$$\beta^*_{ji}(\mathbf{x}, t) = [u_i(\mathbf{x}, t)]\, \nu_j(\mathbf{x})\delta(\mathbf{A} - \mathbf{x}), \tag{2.8}$$

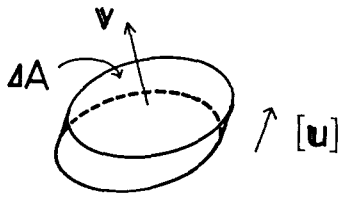

Fig. 1. A microcrack which is modeled as a dislocation source with a fault surface ΔA, a unit surface normal vector ν and a displacement discontinuity $[\mathbf{u}]$.

where $\boldsymbol{\nu}(\mathbf{x})$ is the normal to surface A, $\delta(\mathbf{A} - \mathbf{x})$ is two-dimensional delta function on surface A, which is everywhere zero except on surface A. Consequently eigenstrain $\varepsilon_{ij}^*(\mathbf{x}, t)$ due to the discontinuity of displacement can be represented as

$$\begin{aligned} \varepsilon_{ij}^*(\mathbf{x}, t) &= (1/2)(\beta_{ji}^*(\mathbf{x}, t) + \beta_{ij}^*(\mathbf{x}, t)) \\ &= (1/2)([u_i(\mathbf{x}, t)]\, \nu_j(\mathbf{x}) + [u_j(\mathbf{x}, t)]\, \nu_j(\mathbf{x}))\, \delta(\mathbf{A} - \mathbf{x}). \end{aligned} \tag{2.9}$$

The deformation moment tensor is, from (2.3),

$$D_{jk}(\mathbf{x}, t) = C_{jkmn}[u_m(\mathbf{x}, t)]\, \nu_n(\mathbf{x})\, \Delta A, \tag{2.10}$$

by using $\int_V \delta(\mathbf{A} - \mathbf{x})\, \mathrm{d}V(\mathbf{x}) = \int_A \mathrm{d}S(\mathbf{x})$, where ΔA is the area of surface A. This $D_{jk}(\mathbf{x}, t)$ is called a seismic moment tensor in seismology [15].

For isotropic materials, we have, from (2.4),

$$D_{jk}(\mathbf{x}, t) = (\lambda[u_m]\, \nu_m \delta_{jk} + \mu\, ([u_j]\, \nu_k + [u_k]\, \nu_j))\, \Delta A. \tag{2.11}$$

Substituting (2.11) into (2.6), we can calculate three invariants J_1, J_2 and J_3, and obtain three eigenvalues $D^{(1)}$, $D^{(2)}$ and $D^{(3)}$ from (2.7) as

$$\begin{aligned} D^{(1)} &= ((\lambda + \mu)\, [u_m]\, \nu_m + \mu[u]))\, \Delta A, \\ D^{(2)} &= \lambda[u_m]\, \nu_m \Delta A, \\ D^{(3)} &= ((\lambda + \mu)\, [u_m]\, \nu_m - \mu[u]))\, \Delta A, \end{aligned} \tag{2.12}$$

where $[u]$ is defined as $[u] = ([u_m][u_m])^{1/2}$. Three eigenvectors $\mathbf{x}^{(1)}$, $\mathbf{x}^{(2)}$ and $\mathbf{x}^{(3)}$ are respectively represented as

$$\begin{aligned} x_i^{(1)} &= [u_i] + [u]\, \nu_i \\ x_i^{(2)} &= \varepsilon_{ijk}[u_j]\, \nu_k \\ x_i^{(3)} &= [u_i] - [u]\, \nu_i \end{aligned}$$

where ε_{ijk} is the permutation tensor. This result shows that $\mathbf{x}^{(1)}$ is the vector in the direction of isometric angle between $[\mathbf{u}]$ and $\boldsymbol{\nu}$, $\mathbf{x}^{(2)}$ is the vector in the direction normal to the plane given by $[\mathbf{u}]$ and $\boldsymbol{\nu}$, and $\mathbf{x}^{(3)}$ which is on the plane given $[\mathbf{u}]$ and $\boldsymbol{\nu}$ is normal to $\mathbf{x}^{(1)}$ as shown in Fig. 2. Consequently the generation of displacement discontinuity $[\mathbf{u}]$ on the surface A with the normal $\boldsymbol{\nu}$ is equivalent to the generation of moment with magnitude $D^{(1)}$, $D^{(2)}$ and $D^{(3)}$, and with direction $\mathbf{x}^{(1)}$, $\mathbf{x}^{(2)}$ and $\mathbf{x}^{(3)}$ respectively, which is called a vector dipole which has the same direction of arm and force. Using the trace and/or eigenvalues of moment tensor, the volume ΔV of microcrack can be represented as

$$\begin{aligned} \Delta V &= [u_m]\, \nu_m \Delta A \\ &= D_{ii}/(3\lambda + 2\mu) \end{aligned}$$

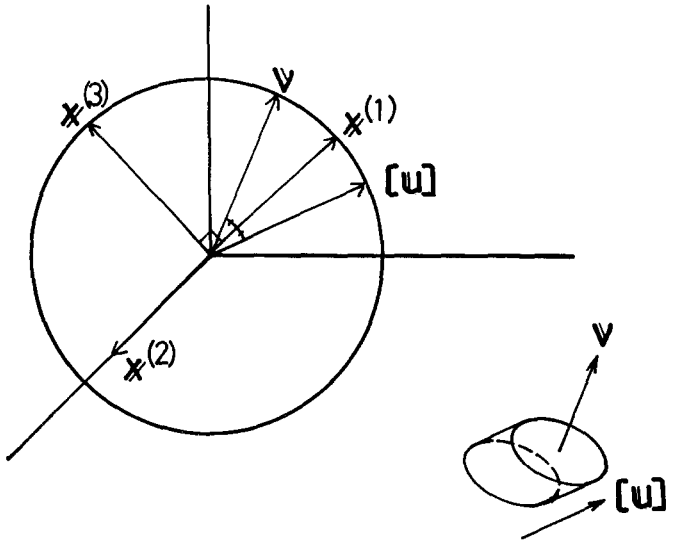

Fig. 2. The eigenvectors $\mathbf{x}^{(1)}$, $\mathbf{x}^{(2)}$ and $\mathbf{x}^{(3)}$ of the microcracking.

$$= (D^{(1)} + D^{(3)})/2(\lambda + \mu)$$

$$= D^{(2)}/\lambda. \tag{2.14}$$

Denoting the angle between [**u**] and $\boldsymbol{v}$ by θ, we have

$$\cos\theta = [u_m]\, v_m/[u]$$

$$= 2\mu D^{(2)}/\lambda(D^{(1)} - D^{(3)}).$$

Thus the quantities ΔV and $\cos\theta$, which characterize microcracking, are represented by the eigenvalues.

Assuming that a microcrack is a disc-like crack subject to a normally applied stress σ, we can state the crack volume as [27]

$$\Delta V = 16a^3\sigma(1 - \nu^2)/3E, \tag{2.16}$$

where a is the crack radius, E is the Young's modulus, and ν is the Poisson's ratio. The crack radius a is, from (2.14) and (2.16),

$$a = (3(1 - 2\nu)D_{ii}/16(1 - \nu^2)\sigma)^{1/3}. \tag{2.17}$$

2.3. AE measurement

The detected signals of acoustic emission are generally different from the displacement field because of the response function of the measuring system. Denoting the response function in the i-direction at the position $\mathbf{x}$ on the surface by $S_i(\mathbf{x}, t)$, the detected signals $V(\mathbf{x}', t)$ due

to moment tensor $D_{jk}(\mathbf{x}, t)$ can be expressed as, from (2.2), [11]

$$V(\mathbf{x}', t) = S_i(\mathbf{x}', t) * G_{ij,k}(\mathbf{x}', \mathbf{x}, t) * D_{jk}(\mathbf{x}, t). \tag{2.18}$$

3. Experiment

Figure 3 shows the block diagram of the multichannel AE detection and recording system. The transducers P50 have a piezoelectric element of about 1 mm and a broad-band response up to a 2 MHz. The output from each transducer was amplified 20 dB by the preamplifier BX31 with a frequency response of DC-70 MHz and then digitized and stored by the wave memory AE9620 with a sampling rate of 10 MHz, resolution of 10 bits and the record length of 1024 points. Data from the wave memory were transferred via GP-IB interface and stored on magnetic disc by a HP216 computer.

An AE analyzer PAC3401 was also used to measure the conventional AE parameters such as events, peak amplitude and energy counts. The output from the transducer R15 with 150 kHz resonance was amplified 40 dB by the preamplifier with a frequency response of 100–300 kHz and fed into the AE analyzer PAC3401. The conventional AE parameters were stored on magnetic disc with the external parameters of load and COD.

The experiment was performed using a standard compact tension specimen of 25 mm thickness. The material was an ASTM A470 steel of which the chemical composition and mechanical properties are given in Table 1. Samples were embrittled by isothermal ageing

Table 1. The chemical composition and mechanical properties of the ASTM A470 steel

Chemical composition (wt %)

C	Si	Mn	P	S	Cu	Cr	Ni	Mo	V
0.29	0.31	0.74	0.006	0.003	0.03	1.12	0.39	1.16	0.26

Mechanical properties

σ_{ys} (MPa)	σ_b (MPa)	δ (%)	ϕ (%)
616	786	20	54

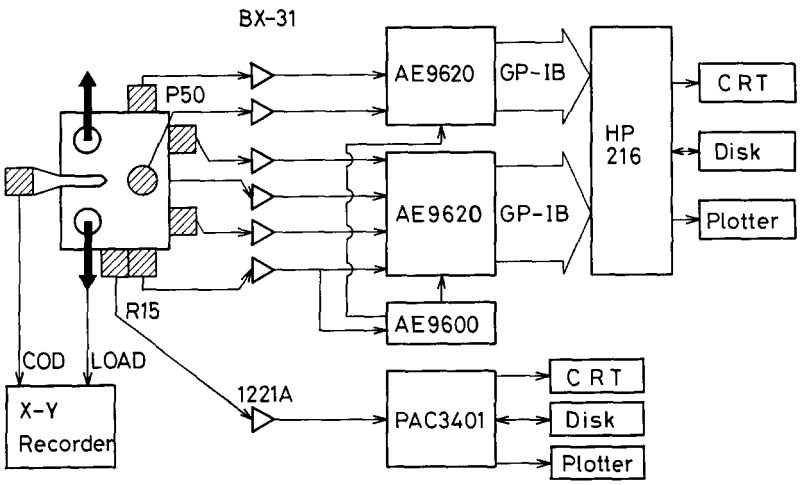

Fig. 3. The block diagram of the acoustic emission measuring system.

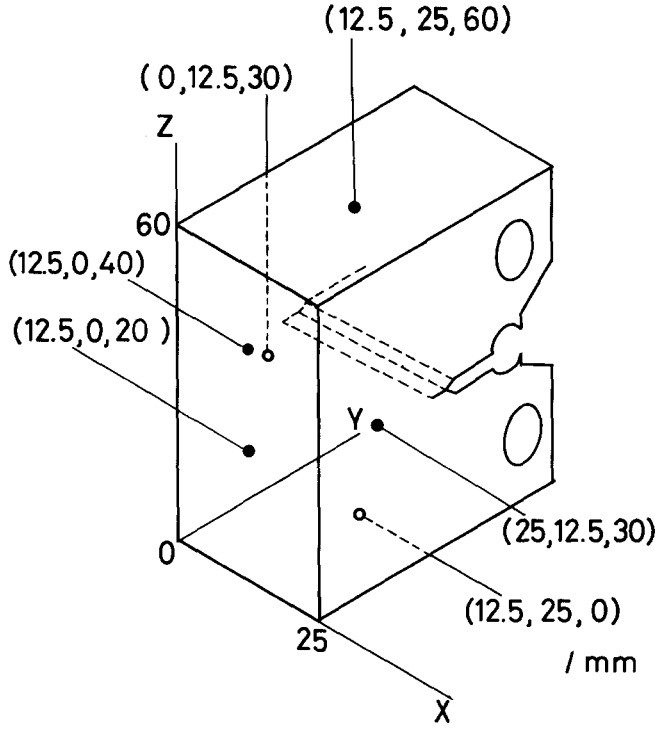

Fig. 4. Geometry of a compact tension specimen and the configuration of six P50 acoustic emission transducers.

at 600° C for times up to 1000 h and were oriented in the RL direction. Prior to fracture toughness tests with AE measurement system, a fatigue pre-crack was introduced.

Fracture toughness tests were carried out at a crosshead speed of 0.5 mm/min and acoustic emission data were recorded during testing. Six P50 transducers were attached to the specimen in the positions shown in Fig. 4.

4. Results

4.1. Fracture toughness test and AE characteristics

Figure 5 shows the load - COD curve and AE total events, total energy data by PAC3401. Fracture toughness K_Q derived from ASTM standard E399 was 60 $MNm^{-3/2}$. There was a rapid increase in both AE total events and energy at about 50 percent loading level of ultimate tensile load.

4.2. Three-dimensional source location

Accurate source location is required in order to understand fracture processes. The location of each source event is determined by measuring the differences in P-wave arrival time between two transducers [19]. Suppose that Δt_{ij} is the difference in the P-wave arrival time between i-th and j-th transducers. Let $\mathbf{r}^i$ denote the transducer positions ($1 \leqslant i \leqslant P$) and $\mathbf{r}$ denote the location of the source, when P is the total number of channels.

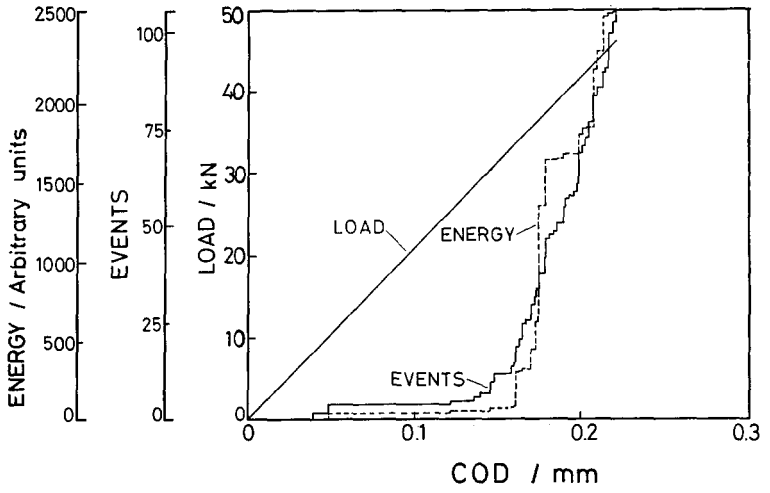

Fig. 5. The load-crack opening displacement (COD) curve with acoustic emission events and energy during the fracture toughness test of the ASTM A470 steel.

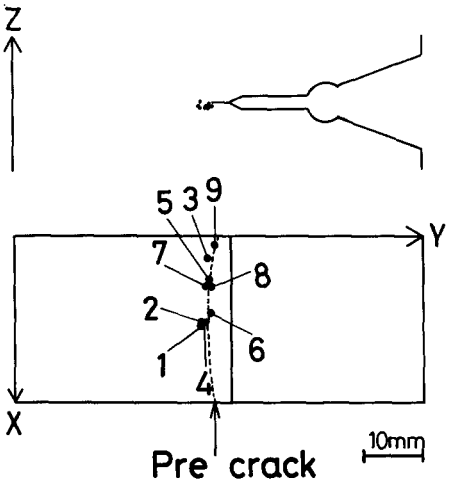

Fig. 6. The location results of acoustic emission sources during the fracture toughness test of ASTM A470 steel.

We can represent the equation for source location as

$$\alpha \Delta t_{iP} = |\mathbf{r} - \mathbf{r}^i| - |\mathbf{r} - \mathbf{r}^P|, \quad 1 \leqslant i \leqslant P - 1, \tag{4.1}$$

where α is the longitudinal velocity (5700 m/s in this material). If $P \geqslant 4$, then a nonlinear least-square method can be used to solve (4.1) for source location $\mathbf{r}$ (see the Appendix). Figure 6 shows the data plotted in projection of the xz and yz planes. The experimental error on each coordinate is estimated to be approximately 1 mm. It can be seen from Fig. 6 that source events are generated along the fatigue pre-crack approximately horizontally.

4.3. Calculation of Green's function

The analytical [20], experimental [11] or numerical researches on Green's function of media have been investigated. However, the Green's function which has the complex boundary

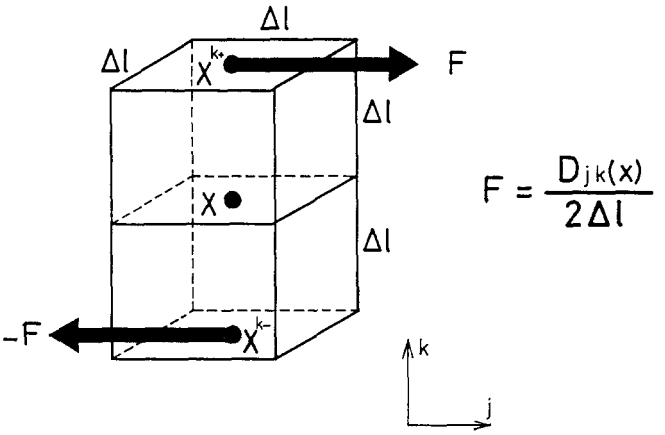

Fig. 7. A component of the moment tensor applied at an AE source position for the finite difference method.

conditions can be obtained only by the numerical simulation method. We simulate the dynamic Green's function of 1TCT specimen by a finite difference method [21]. Effect of the pins and pin-holes can be neglected near the *P*-wave arrival. The finite difference formulations for equations of motion are derived by replacing the derivatives of the equation of motion with central differences for inner points. The one-sided approximations of Alterman and Lowenthal [22] are used for the free boundary conditions. In order to produce the moment $D_{jk}(\mathbf{x}, t)$ with force in the j-direction and arm in the k-direction at inner position $\mathbf{x}$, we apply a single couple with magnitude of $D_{jk}(\mathbf{x}, t)/2\Delta l$ in the k-direction at both forward and backward points of $\mathbf{x}$ in the j-direction (Fig. 7). We calculate the response functions at each transducer's position due to nine components of moment tensor at the obtained location of each source, where we use the mesh size $\Delta l = 0.5\,\text{mm}$, the increment in time $\Delta t = 0.05\,\mu\text{s}$, Lamé's constants $\lambda = 1.07 \times 10^{11}\,\text{Pa}$, $\mu = 7.67 \times 10^{10}\,\text{Pa}$, the mass density $\varrho = 7.87 \times 10^{3}\,\text{kg m}^{-3}$, the step-like function with a rise time $Rt = 0.5\,\mu\text{s}$ and the magnitude of moment $D_0 = 1\,\text{Nm}$. For example, Fig. 8 shows the response at the transducer's position on the upper surface of the specimen due to the source event of location No. 1 in Fig. 6.

4.4. Response function of measuring system

The transducers and measuring system were calibrated using a breaking pencil lead [23, 24]. Before the fracture toughness testing, the waveform data due to the breaking pencil lead at the surface of the specimen were recorded. The Green's function corresponding to the breaking pencil lead was calculated by a finite difference method. Then the response function of the measuring system was obtained from the result of the deconvolution with the known source function of the breaking pencil lead [24] and the above Green's function.

4.5. Deconvolution with multiple Green's functions

Assuming that the components of the microcracking moment tensor have the same time function $T(t)$, (2.18) is written as

$$v^p(t) = c_r H_r^p(t) * T(t), \quad 1 \leqslant p \leqslant P. \tag{4.2}$$

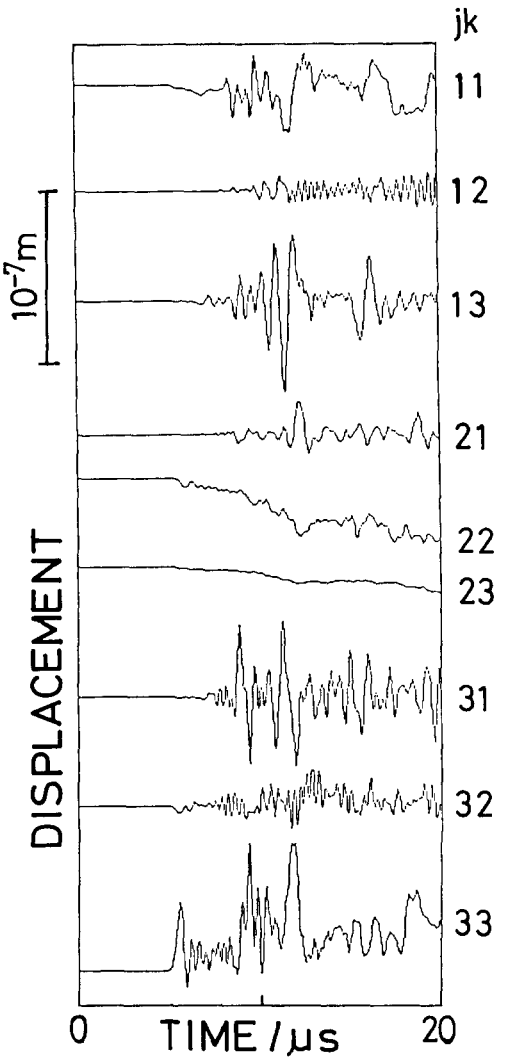

Fig. 8. The example of the response function $G_{ij,k}$ at the position of the transducer (12.5, 25, 60) in Fig. 4 which is simulated by the finite difference method.

The problem of source characterization is then to simultaneously determine $T(t)$ and c_r $(1 \leqslant r \leqslant R)$, given $v^p(t)$ and $H_r^p(t)$ over a finite time interval [25]. Let N be the value of n which corresponds to the maximum time for which $v^p(t)$ and $H_r^p(t)$ are specified. The convolution integral in (4.2) reduces to a summation as

$$v^p(n) = \sum_{k=1}^{N} c_r H_r^p(n - k + 1) T(k) \Delta t, \quad 1 \leqslant n \leqslant N. \tag{4.3}$$

We develop the iterative algorithm to solve this nonlinear equation by using the method in the Appendix as follows:

(i) The c_r coefficients and $T(n)$ are set to nonzero initial values.

(ii) Using these c_r, the $T^p(n)$ $(1 \leqslant p \leqslant P)$ are calculated from (4.3) by using the method in the Appendix.

(iii) These $T^q(n)$ $(1 \leqslant q \leqslant P)$ are used to calculate the improved c_r^{pq} from (4.3).

$$D_{jk}(t) = \overline{D} \begin{pmatrix} 0.41 & 0.04 & -0.22 \\ & 0.17 & 0.01 \\ \text{sym.} & & 1 \end{pmatrix} T(t)$$

$$\overline{D} = 5.02 \times 10^{-4}\ \text{Nm}$$

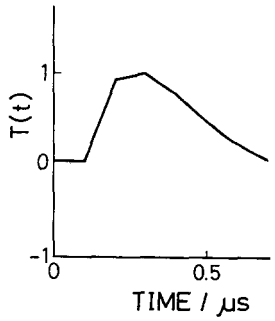

Fig. 9. The obtained result of moment tensor components and the time function due to microcracking in the ASTM A470 steel.

(iv) The more improved c_r, $T(n)$ are obtained by averaging.

(v) These procedures of alternately calculating c_r and $T(n)$ can be continued until the c_r and $T(n)$ converge to fixed values.

Moment tensor D_{jk} was determined by the deconvolution method using 60 time points from P-wave arrival. Figure 9 shows an example of moment tensor D_{jk}.

5. Discussion

5.1. Characteristics of microcracking – size, fracture mode, inclination of fracture surface and mean nucleation rate

As shown in Fig. 9, a microcrack is generated with a rise time of about 0.3 μs. Applying the method of the Appendix to (2.11), the displacement discontinuity [**u**] and the normal $\boldsymbol{\nu}$ were obtained from the determined moment tensor D_{jk}. Figure 10 indicates that the inclination of the microcrack plane to the main crack surface was 15 deg and the inclination of the microcrack plane to the direction of the displacement discontinuity was 58 deg. This result demonstrates that a microcracking occurs in mixed mode of tensile and shear. A crack radius a is calculated from (2.17) by assuming $\sigma = 3\sigma_{ys}$. Table 2 shows that the value of radius a is estimated as 26 to 50 μm. In any case, quantitative evaluation of each microcrack is possible by using the obtained moment tensor.

5.2. Accuracy of the three-dimensional location and plastic zone

AE sources were generated along the fatigue pre-crack. The errors of source location are given by a sampling rate, positions of transducers and dimensions of transducers. A

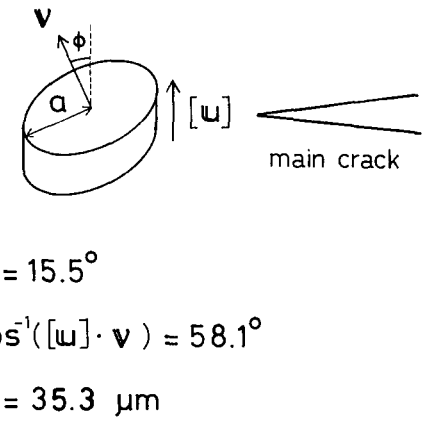

Fig. 10. The results of the inclination of the microcrack plane with respect to the main crack surface ϕ, the inclination of the microcrack plane to the direction of the displacement discontinuity **[u]**, and the radius of the microcrack a.

Table 2. The results of the normalized moment tensor component, the nucleation time and the radius of each microcrack in the ASTM A470 steel

No.	$\bar{D}/10^{-3}$ Nm	$\Delta t/\mu$s	a/μm
1	0.50	0.2	35
2	0.39	0.3	32
3	0.43	0.2	33
4	1.2	0.4	46
5	1.5	0.7	50
6	0.22	0.2	26
7	0.33	0.2	30
8	1.1	0.4	44

sampling rate of 10 MHz and a longitudinal velocity of 5700 m/s in this material give the maximum error of about 0.6 mm in source location. Although the size of the piezoelectric element is about 1 mm, the error of positions in attachment of transducers is smaller than this one. The compact tension specimen used in this experiment was convenient for source location in the view of wide receiving of radiation. Consequently, the maximum total error of AE source location is presumed about 0.6 mm. We can obtain the source location using more than four channel data of AE waveform. We cannot recognize the difference between the results of source location using six channel data of AE waveform and those using four channel data. This fact shows that the maximum total error of AE source location is relatively small.

All of the sources were located within 1 mm of the crack tip. The dimension of plastic zone was about 0.5 mm, from the results of yield stress 616 MPa and fracture toughness 60 MNm$^{-3/2}$. Thus AE sources were believed to be microcracks in the plastic zone in consideration of error of source location, and so it will be possible to determine the dimension of plastic zone from the results of source location.

Figure 11 shows the macroscopic and microscopic fracture surface. The quasi-cleavage facets, whose sizes were about 60 μm, were observed at the location of sources and the size of the quasi-cleavage facets agreed well with the estimated value of radii from waveform of acoustic emissions on the assumption of disc-like cracks. This result justifies that the generation of microcracks are represented as a point source with displacement discontinuities.

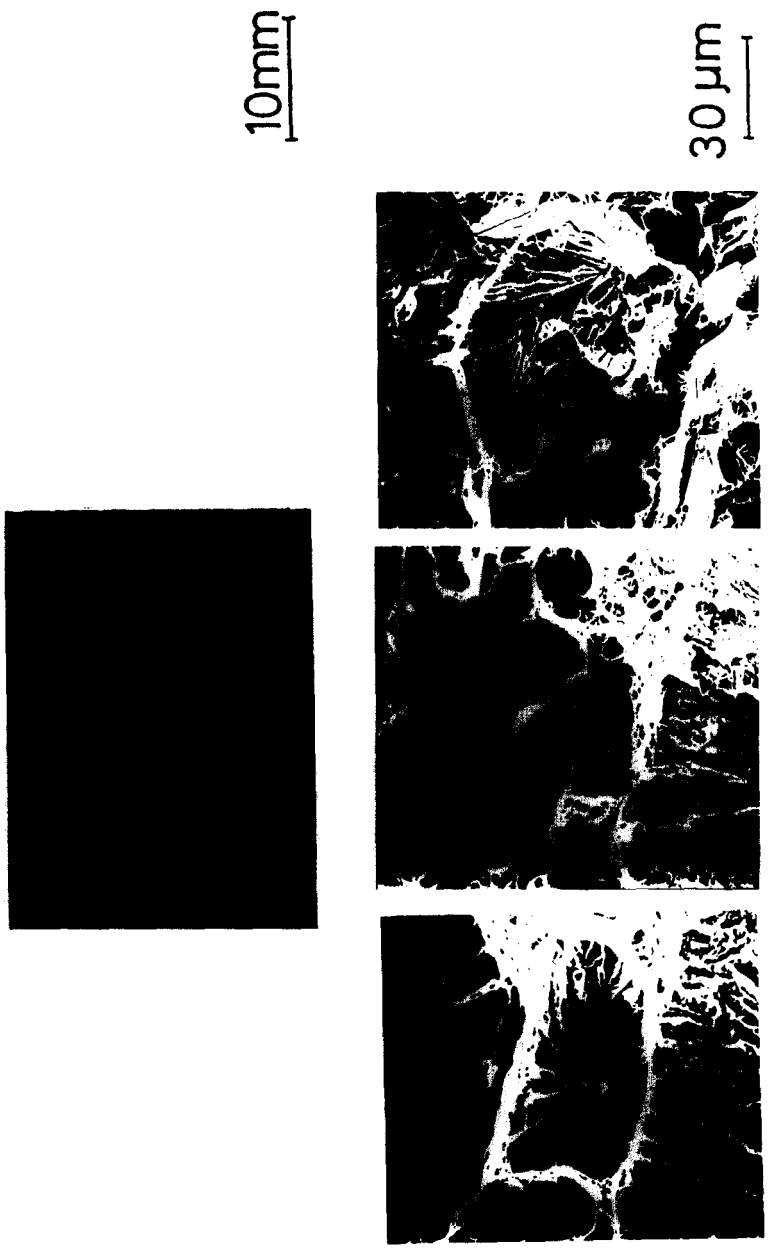

Fig. 11. The macroscopic fracture surface of the ASTM A470 steel and the quasi-cleavage facets along the fatigue pre-crack.

5.3. Dynamic Green's function

In the inverse problem to determine the moment tensor from AE signals, dynamic Green's function of a medium without crack has been used [12]. The microcracks near the main crack as shown in this result, however, influence the dynamic Green's function of a medium. Thus, we should use the dynamic Green's function with the main crack in the material. In the case of microcracking near the main crack it would overestimate the moment tensor components to use the dynamic Green's function of a half space of half plate [26]. And it would increase the error of ratio between each component and give an inexact fracture mode. It was convenient to use our dynamic Green's function of a compact tension specimen with a main crack in accuracy of moment tensor components. In the calculation of dynamic Green's function more computer memory is saved by the finite difference method than by the finite element method.

5.4. Size and fracture mode

Figure 10 shows that this analyzed microcrack is a crack with mixed fracture mode, which has more shear components than tensile. As no other experimental procedure to determine the fracture mode of microcracking is available, we cannot prove this result. All the detected signals, which are used in this analysis, have the same radiation pattern of longitudinal wave. In such cases fracture mode of microcracking has been presumed to be a mode I, that is, a tensile type on the consideration of radiation pattern of AE waveform [8, 11]. Thus, exact fracture mode of microcracking cannot be easily obtained, but the analysis with this assumption gives good estimates in the size of microcrackings.

5.5. Error of the estimated moment tensor

The reason for error of the obtained moment tensor components can be referred to calibration of measuring system, dynamic Green's function of medium and deconvolution method. The error of calibration of measuring system directly influences the moment tensor components. As we used dynamic Green's function of compact tension specimen with a main crack for determination of moment tensor components, the error of dynamic Green's function can be estimated to be smaller than the other Green's function. It is well known that solution by deconvolution method has less convergence, and deconvolution in the presence of noise expands the error of solutions [25]. Thus, all the errors in the moment tensor components could probably be estimated at about 10 percent. Although the error in the volume of microcrack is 10 percent, the error in the radius of microcrack, obtained from (2.17), is reduced to about 3 percent. However, the maximum errors in the fracture mode are not clear because errors in the fracture mode can be produced from noise.

5.6. Quasi-cleavage facet

By the results of source location and deconvolution and the observation of fracture surface by scanning electron microscope, AE sources in this experiment were identified as the quasi-cleavage facets with sizes of about 60 μm. Although waveform analysis was performed by using AE signals with relatively large amplitude, small microcracks less than 60 μm could be analyzed. However, those microcracks of about 60 μm are likely to dominate the fracture process, that is, these microcracks will become the origin for unstable fracture.

6. Conclusions

In this paper we presented a theoretical consideration for an infinitesimal deformation and made clear the physical meaning of microcracking, which is a typical example of an infinitesimal deformation, in accordance with the method of micromechanics. We also developed the experimental analysis method by using AE signals in order to evaluate this microcracking quantitatively. Applying this method to fracture toughness testing of A470 steel, the following conclusions can be drawn.

(1) The method expressing an infinitesimal deformation in materials as a deformation moment tensor or an eigenstrain tensor has been proposed and the physical meaning of this moment tensor due to the nucleation of microcracking has been made clear.

(2) New experimental and analysis system due to AE source characterization, which can determine the moment tensor components in microcracking, was developed. This method is remarkable for the dynamic Green's function of finite media by finite difference computer simulation and for the iterative deconvolution with multiple Green's function.

(3) Three-dimensional location can clearly show that AE sources are located in the plastic zone near the pre-crack tip.

(4) From the obtained result of moment tensor, size, inclination of microcrack surface and fracture mode of each microcrack were quantitatively evaluated.

(5) The observation by scanning electron microscope verified that these AE sources are identified as the quasi-cleavage facets along the fatigue pre-crack, which have a size of 50–100 μm. As a microfracture process of this material it can be expected that those facets nucleate at 50 percent of the ultimate failure load and the unstable fracture starts after these several facets have nucleated. This result justifies that generation of microcracks are represented as a point source with displacement discontinuities.

It can be concluded that this developed method, which can evaluate quantitatively location, fracture mode and size of microcracks, is a powerful tool as a new experimental technique for understanding microcracks.

References

1. J.F. Knott, in *Fundamentals of Fracture Mechanics*, Butterworths, London (1973).
2. G.T. Hahn and A.R. Rosenfield, *Metallurgical Transactions* 6A (1975) 653–670.
3. S.P. Rawal and J. Gurland, *Metallurgical Transactions* 8A (1977) 691.
4. G. Green and J.F. Knott, *Transactions of the ASME* H 98 (1976) 37.
5. R.O. Ritchie, J.F. Knott and J.R. Rice, *Journal of the Mechanics and Physics of Solids* 21 (1973) 395–410.
6. A.G. Evans and R.M. Cannon, *Acta Metallurgica* 34 (1986) 761–800.
7. A.G. Evans and K.T. Faber, *Journal of the American Ceramic Society* 67 (1984) 255–260.
8. T. Kishi, S. Wakayama and S. Kohara, in *Fracture Mechanics of Ceramics*, Vol. 8, Plenum Press (1986) 85–100.
9. T. Mura, in *Micromechanics of Defects in Solids*, Martinus Nijhoff Publishers, The Hague (1982).
10. H.N.G. Wadley, C.B. Scruby and G. Shrimpton, *Acta Metallurgica* 29 (1981) 399–414.
11. T. Kishi and T. Ohira, *Transactions of Japan Institute of Metals* 24 (1983) 255–263.
12. C.B. Scruby, K.A. Stacey and G.R. Baldwin, *Journal of Physics* D19 (1986) 1597–1612.
13. K.Y. Kim and W. Sachse, *International Journal of Fracture* 31 (1986) 211–231.
14. P. Fleischmann and P. Rouby, in *Progress in Acoustic Emission II*, The Japanese Society for Non-Destructive Inspection (1984) 114–124.
15. K. Aki and P.G. Richards, in *Quantitative Seismology*, Vol. I, W.H. Freeman and Company, San Francisco (1980).

16. M. Ohtsu and K. Ono, *Journal of Acoustic Emission* 3 (1984) 27–40.
17. T. Mura, *Bulletin of the American Physical Society* 6 (1961) 521.
18. R. Burridge and L. Knopoff, *Bulletin of the Seismological Society of America*, 54 (1964) 1875–1888.
19. C.B. Scruby and G.R. Baldwin, *Journal of Acoustic Emission* 3 (1984) 182–188.
20. A.N. Ceranoglu and Y.H. Pao, *Journal of Applied Mechanics* 48 (1981) 125–147.
21. Y. Fukunaga, M. Enoki and T. Kishi, to be published.
22. Z.S. Altermann and D. Lowenthal, *Geophysical Journal of the Royal Astronomical Society* 20 (1970) 101–126.
23. N.N. Hsu, J. Simmons and H.C. Hardy, *Materials Evaluation* 35 (1977) 100–106.
24. N. Ohisa and T. Kishi, in *Proceedings of the 1982 Joint Conference on Experimental Mechanics*, Society for Experimental Stress Analysis (1982) 359–364.
25. J.E. Michaels and Y.H. Pao, *Journal of the Acoustical Society of America* 77 (1985) 2005–2011.
26. J.D. Achenbach, K. Hirashima and K. Ohno, *Journal of Sound and Vibration* 89 (1983) 523–532.
27. J.W. Hutchinson, *Acta Metallurgica* 35 (1987) 1605–1619.

Appendix

The nonlinear least square method

Now consider the nonlinear multi-dimensional equations in respect to x_j ($1 \leqslant j \leqslant n$) as

$$f_i(\mathbf{x}) = 0, \quad 1 \leqslant i \leqslant m. \tag{A-1}$$

Let F be the least squares error as

$$F = f_i f_i. \tag{A-2}$$

Let $\mathbf{x}^k$ be the k-th value of $\mathbf{x}$ in iteration and $\Delta\mathbf{x}^k$ be the difference between $\mathbf{x}^{k+1}$ and $\mathbf{x}^k$ as

$$\Delta x_j^k = x_j^{k+1} - x_j^k. \tag{A-3}$$

The conditions, $\partial F^{k+1}/\partial \Delta x_1^k = 0$, give rise to a system of equations for the Δx_j^k, that is,

$$a_{il}^k a_{ij}^k \Delta x_j^k = -a_{il}^k f_i^k, \tag{A-4}$$

where a_{ij}^k is the Jacobian of $f_i^k(\mathbf{x})$. This system of equations, called a Newton–Gauss equation, can be solved for Δx_j^k. It was improved by Levenberg and Marquardt as

$$a_{il}^k a_{ij}^k \Delta x_j^k + v^2 \delta_{ij} \Delta x_j^k = -a_{il}^k f_i^k, \tag{A-5}$$

where v, called Marquardt's number, is changed so that convergence is reached in a reasonable number of iterations. This procedure of calculation Δx_j^k can be continued until x_j^k converge to fixed values.

Résumé. On propose une méthode de représentation d'une déformation générale infinitésimale sous forme d'une tenseur de moment de déformation et on clarifie la signification physique de ce tenseur dans le cas d'une microfissuration. Grâce à un développement d'un système de mesure et d'analyse de la forme d'onde en émission acoustique, on peut déterminer par voie expérimentale les composantes du tenseur de moment correspondant à une microfissuration. La méthode est remarquablement adaptée à l'évaluation du tenseur de moment associé à une fonction dynamique du Green pour les milieux finis, en utilisant une simulation par calcul, appliquée à la méthode des différences finies et à une decompositées par itération d'une fonction multiple de Green.

En appliquant la méthode aux essais de tenacité à la rupture de l'acier ASTM A470, on obtient à l'aide d'une analyse des ondes d'émissions acoustiques sur six canaux, le tenseur de moment relatif à une facette en quasi-clivage dans la zone plastique au voisinage de l'extrémité d'une préfissure. En outre, le tenseur de moment permet d'estimer la localisation sur trois dimensions de ces microfissures, leur taille quantitative et le mode de rupture.